Temperature versus Sm concentration phase diagram and quantum criticality in the correlated electron system $Ce_{1-x}Sm_xCoIn_5$

N. Pouse,[1,2] S. Jang,[2,3,*] B. D. White,[1,2,†] S. Ran,[1,2,‡] R. B. Adhikari,[4] C. C. Almasan,[4] and M. B. Maple[1,2,3,§]

[1]*Department of Physics, University of California, San Diego, La Jolla, California 92093, USA*

[2]*Center for Advanced Nanoscience, University of California, San Diego, La Jolla, California 92093, USA*

[3]*Materials Science and Engineering Program, University of California, San Diego, La Jolla, California 92093, USA*

[4]*Department of Physics, Kent State University, Kent, Ohio 44242, USA*

(Received 16 April 2018; revised manuscript received 18 June 2018; published 28 June 2018)

We report electrical resistivity, magnetization, and specific heat measurements on the correlated electron system $Ce_{1-x}Sm_xCoIn_5$ ($0 \leqslant x \leqslant 1$). Superconductivity (SC) in the heavy-fermion compound $CeCoIn_5$, which is suppressed with increasing Sm concentration x, and antiferromagnetic (AFM) order of $SmCoIn_5$, which is suppressed with decreasing x, converge near a quantum critical point at $x_{QCP} \approx 0.15$, with no indication of coexistence of SC and AFM in the vicinity of the QCP. Non-Fermi-liquid (NFL) behavior is observed in the normal-state electrical resistivity, $\rho(T)$, and specific heat, $C(T)$, in the vicinity of the QCP; e.g., the coefficient and the exponent of the power-law T dependence of $\rho(T)$ exhibit pronounced maxima and minima, respectively, at x_{QCP}, while $C(T)/T$ exhibits a logarithmic divergence in T at x_{QCP}. A low-temperature upturn in $\rho(T)$ develops in the range $0.70 \leqslant x \leqslant 0.85$ which is reminiscent of a single impurity Kondo effect, suggesting that Sm substitution tunes the relative strength of competing Kondo and Ruderman-Kittel-Kasuya-Yosida energy scales. The suppression of SC with increasing x is probably associated with the exchange interaction between the Ce quasiparticles involved in the superconductivity and the magnetic moments of the Sm ions.

DOI: 10.1103/PhysRevB.97.235149

I. INTRODUCTION

Quantum criticality has been an important and fascinating area of correlated electron research due in large part to its presence in disparate classes of materials including cuprates and iron pnictide high-temperature superconductors, as well as lanthanide- and actinide-based heavy-fermion (HF) metals [1]. A quantum critical point (QCP) emerges when a second-order phase transition is suppressed to zero temperature by tuning nonthermal control parameters such as chemical composition, applied pressure, or magnetic field, frequently yielding an observable superconducting state [2]. The proximity of superconductivity to magnetism in these materials has led to an ongoing debate about the underlying mechanism behind the emergent superconductivity and continues to drive a great deal of research in this area [3]. The HF superconductors $CeTIn_5$ (T = Co, Rh, Ir) are a prototypical class of strongly correlated systems in which unconventional superconductivity (SC) emerges in close proximity to an antiferromagnetic (AFM) QCP [3–6].

The compound $CeCoIn_5$ is a d-wave superconductor [7–10] that has provided an opportunity to study the effects of impurities, either magnetic or nonmagnetic, on an unconventional superconductor. The compound $SmCoIn_5$ is isostructural with $CeCoIn_5$, but undergoes three successive phase transitions [11] and has not been found to exhibit superconductivity under ambient or applied pressure up to 8 GPa [12]. This is in contrast with the related compound $PuCoIn_5$ in which superconductivity was observed [13]; $PuCoIn_5$ and $SmCoIn_5$ have the same crystal structure and Pu^{3+} shares the same f-electron shell configuration as Sm^{3+}.

Our study of the system $Ce_{1-x}Sm_xCoIn_5$ reported herein was motivated by a series of studies on the system $Ce_{1-x}Yb_xCoIn_5$ [14,15]. Ytterbium, which can have the same valence states as Sm (2+, 3+), was found to display valence fluctuations when substituted into the Ce site, while Ce remained trivalent [14,16]. The Yb valence decreases rapidly from 3+ at low x until stabilizing at 2.3+ for $x >$ 0.07 [16]. The decrease in Yb valence in $Ce_{1-x}Yb_xCoIn_5$ is accompanied by other anomalous phenomena at $x = 0.07$, such as suppression of the quantum critical field, H_{QCP} [17], a Fermi-surface reconstruction [18], and a possible crossover from a nodal to nodeless superconducting energy gap [19]. This last result was observed in measurements of the London penetration depth, $\lambda(T)$ [19]; although, recent thermal conductivity measurements do not show this change in the superconducting energy gap [20]. This nodeless superconductivity has been explored by a composite pairing scenario in which a fully gapped d-wave molecular superfluid of composite pairs form

*Present address: Department of Physics, University of California, Berkeley, California 94720.

†Present address: Department of Physics, Central Washington University, 400 East University Way, Ellensburg, Washington 98926-7442.

‡Present addresses: Center for Nanophysics and Advanced Materials, Department of Physics, University of Maryland, College Park, MD 20742; NIST Center for Neutron Research, National Institute of Standards and Technology, 100 Bureau Drive, Gaithersburg, MD 20899.

§Corresponding author: mbmaple@ucsd.edu

[21]. By substituting Sm into the Ce site in this study, we were interested in seeing whether we could observe some of the same phenomena reported in the Yb-substituted system [22,23].

Our measurements of the specific heat of $SmCoIn_5$ indicate that there are two additional phase transitions besides AFM order at $T_N \sim 11.6$ K, including a first-order transition at 10.2 K, and another transition with a smaller feature at 6.0 K. This behavior, with three transitions, is similar to that observed in a previous study of $SmIn_3$ [24]; however, the origin of these additional phase transitions is unknown in $SmCoIn_5$. From μSR measurements on $SmIn_3$, it is suggested that these ordering temperatures are associated with a transition between commensurate and incommensurate AFM states [25], although the signatures of the transitions are qualitatively different when we compare specific heat measurements on $SmCoIn_5$ and $SmIn_3$. Additional experiments such as anomalous x-ray diffraction must be conducted to determine the nature of these transitions. Introducing Ce into $SmCoIn_5$ disrupts the additional phase transitions observed in $SmCoIn_5$ and results in a single, broad transition in the specific heat for concentrations down to $x = 0.175$. On the Ce-rich side of the phase diagram, we

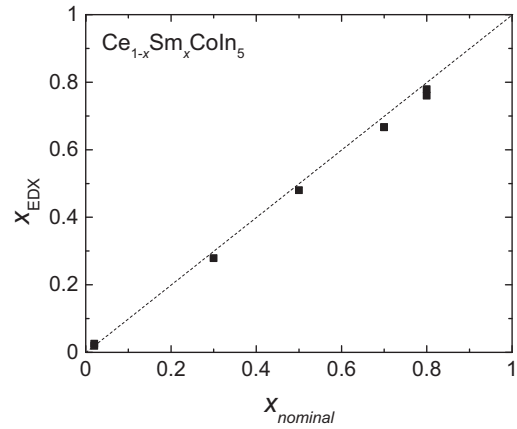

FIG. 1. Energy-dispersive x-ray spectroscopy (EDX) measurements were performed on selected single crystals of $Ce_{1-x}Sm_xCoIn_5$. We observed excellent agreement between the measured and nominal Sm concentrations. EDX measurements were performed at several locations for each sample to evaluate the chemical homogeneity of synthesized single crystals. The dashed line is a guide to the eye.

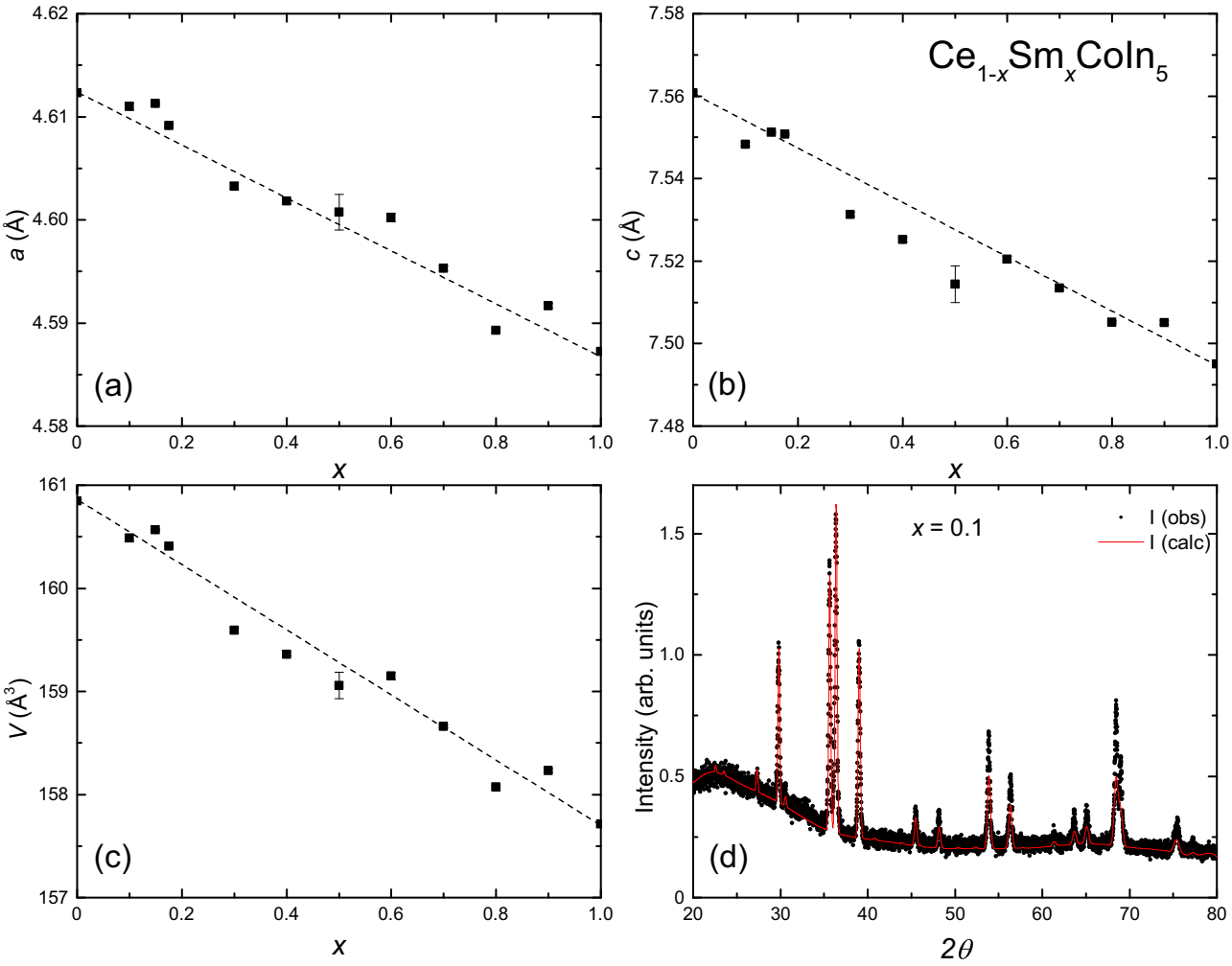

FIG. 2. (a), (b) Lattice constants, a and c, plotted as a function of x, respectively. (c) Volume of the unit cell, V, plotted as a function of x. (d) Representative powder x-ray diffraction pattern for an $x = 0.1$ sample (black circles) and calculated fit from the Rietveld refinement (red line) used to determine the lattice constants a and c. In panels (a)–(c), dashed lines are guides to the eye. Error bars for all concentrations and most are less than or of the order of 10^{-4} Å; however, the $x = 0.5$ sample has a larger error bar of the order of 10^{-3} Å.

find that superconductivity is rapidly suppressed by $x = 0.15$. Electrical resistivity data demonstrate that the Kondo coherence temperature T^* is also suppressed with increasing x. The evolution of SC and AFM order across the $Ce_{1-x}Sm_xCoIn_5$ phase diagram provides information about the interplay of these two phenomena and non-Fermi-liquid (NFL) behavior of the physical properties near a QCP in this system.

II. EXPERIMENTAL DETAILS

Single-crystalline samples of $Ce_{1-x}Sm_xCoIn_5$ were grown using a molten In flux as described in Ref. [26]. The crystal structure was characterized through analysis of powder x-ray diffraction (XRD) patterns collected by a Bruker D8 Discover x-ray diffractometer using a Cu $K\alpha$ source. The chemical composition was investigated by means of energy-dispersive x-ray spectroscopy (EDX) using an FEI Quanta 600 scanning electron microscope equipped with an INCA EDX detector from Oxford Instruments. Four-wire electrical resistivity measurements, $\rho(T)$, were performed from 300 K down to ~ 1.1 K in a pumped ^{4}He Dewar and down to 1.8 K in a Quantum Design Physical Property Measurement System (PPMS) DynaCool. For selected samples, $\rho(T)$ was also measured down to 25 mK in an Oxford Kelvinox-300 ^{3}He-^{4}He dilution refrigerator. Magnetic susceptibility measurements were performed between 300 and 2 K in a Quantum Design Magnetic Property Measurement System equipped with a 7 T superconducting magnet. Specific heat measurements were performed down to 1.8 K in a Quantum Design PPMS DynaCool and down to 0.5 K using a ^{3}He option. All specific heat measurements were made using a standard thermal relaxation technique.

III. RESULTS

A. Crystal structure

EDX measurements were performed on selected single crystals used for measurements in this study; we observed excellent agreement between measured (x_{EDX}) and nominal Sm concentration values (x_{nom}) over the entire range of x as shown in Fig. 1. Deviations from this agreement may represent inhomogeneity within the single crystals being measured by EDX or experimental error from the analysis on Sm concentration. Another plausible explanation is the formation of $SmIn_3$ using excess In from the molten flux melt which would contribute to a Sm deficiency in the single crystals. This explanation is backed by observations in $C(T)$ measurements of rare $Ce_{1-x}Sm_xCoIn_5$ single crystals showing multiple peaks associated with $SmIn_3$ transitions [24]. Crystals exhibiting this behavior were screened; however, this could still account for small deficiencies in Sm which can be manifested in EDX and powder XRD data for the lattice parameters. These results

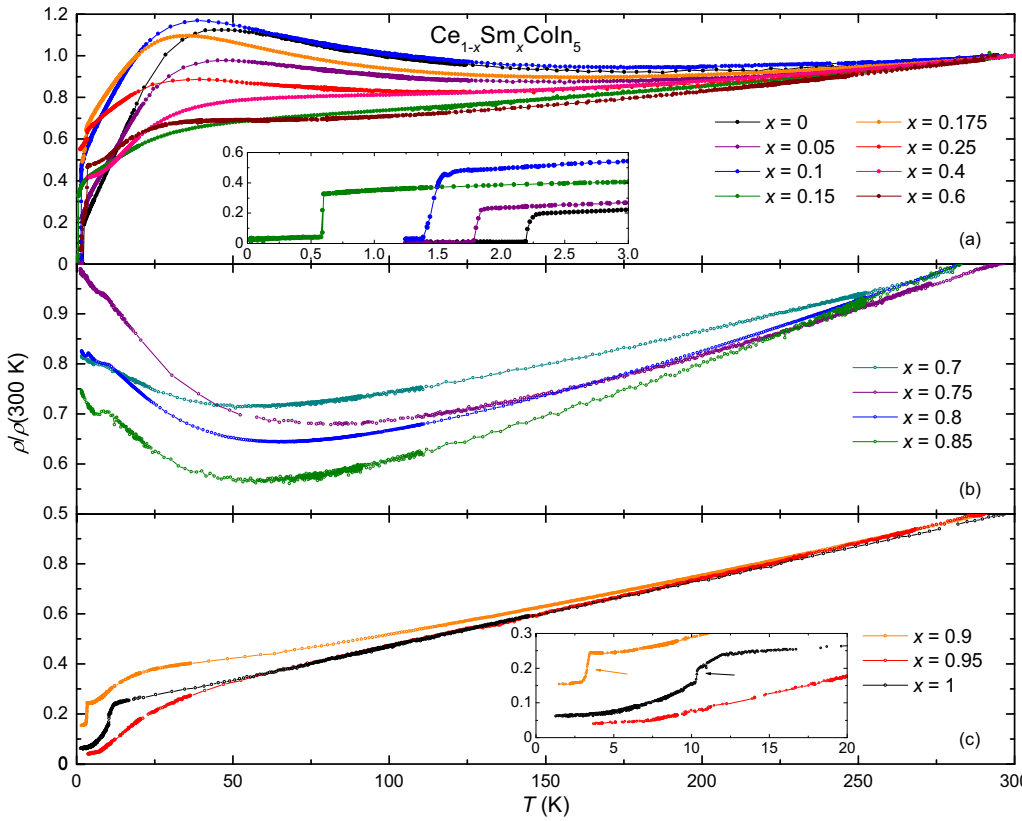

FIG. 3. Electrical resistivity, ρ, normalized by its value at 300 K, plotted vs temperature, T, for $Ce_{1-x}Sm_xCoIn_5$. (a) Samples with low Sm concentration display both a coherence peak associated with the formation of a coherent Kondo lattice and superconductivity (see inset) that is suppressed with increasing x. (b) As x increases above 0.6, we observe a crossover into a single-ion-like Kondo effect in which Ce ions behave as a magnetic impurity in $SmCoIn_5$. (c) On the Sm-rich side of the phase diagram, the only salient feature observed is a sharp, "kneelike" feature consistent with AFM order of the Sm sublattice, as observed previously (see inset) [12].

suggest that there is neither a solubility limit nor a miscibility gap in the $Ce_{1-x}Sm_xCoIn_5$ system.

Rietveld refinements were performed on powder XRD patterns for each sample using GSAS [27] and EXPGUI [28]; the lattice constants are presented in Figs. 2(a) and 2(b), while the unit-cell volume is shown in Fig. 2(c). The $Ce_{1-x}Sm_xCoIn_5$ system exhibits a single tetragonal crystal structure with space group $P4/mmm$ over the entire concentration range. A representative XRD pattern for an $x = 0.1$ sample is displayed in Fig. 2(d). The expected Bragg reflection pattern is shown in red and the measured XRD pattern is displayed as a black scatter plot that overlaps the refined XRD pattern. The agreement between our data and the refinement results was excellent for all samples with typical reduced χ^2 values of less than 5. The lattice constants, a and c, along with the unit-cell volume, V, decrease linearly with increasing Sm concentration which is in agreement with Vegard's law [see Figs. 2(a)–2(c)]. This adherence to Vegard's law suggests that the Sm valence remains constant at 3+ for all concentrations.

B. Electrical resistivity

Electrical resistivity, $\rho(T)$, measurements were performed on selected samples in the $Ce_{1-x}Sm_xCoIn_5$ system, and the data are displayed in Fig. 3. The behavior of $\rho(T)$ evolves with increasing Sm concentration through three distinct regions: low Sm concentrations with $x \leqslant 0.6$ [panel (a)], intermediate region $0.7 \leqslant x \leqslant 0.85$ [panel (b)], and high Sm-concentration region of $x \geqslant 0.9$ [panel (c)]. From published studies, we expect a superconducting transition in $CeCoIn_5$ [3–5] and three successive phase transitions, one of which is AFM, for $SmCoIn_5$ [11,12]. Our data for the parent compounds are consistent with published studies; rare-earth substitution (Sm for Ce or Ce for Sm) away from the Ce- and Sm-based parent compounds suppresses these transitions to lower temperatures.

Upon chemical substitution away from the Ce- and Sm-based end member compounds, both T_N and T_c appear to be suppressed linearly initially (see the phase diagram in Fig. 4); we were unable to observe evidence for coexistence of SC and AFM order in measurements down to ~25 mK at any Sm concentration, x. We note that it was difficult to clearly identify AFM order for some concentrations due to the presence of the coherence peak and the decreasing size of the drop in $\rho(T)$ associated with the onset of the AFM order. Therefore, only electrical resistivity data are used to identify T_c, while T_N is determined from specific heat data that will be discussed below. These results are summarized in the phase diagram in Fig. 4.

As we alloy away from each parent compound, we also observe a change in the interplay between the Ruderman-Kittel-Kasuya-Yosida (RKKY) interaction and the Kondo effect. For $CeCoIn_5$, a coherence peak in $\rho(T)$ associated with the formation of a Kondo lattice involving Ce^{3+} ions is observed. With increasing x, the coherence peak gradually shifts to lower temperature and broadens as seen in Fig. 3(a). The magnitude and position of the peak in $\rho(T)$ associated with Kondo lattice behavior may not evolve smoothly throughout the alloy series due to the influence on the aforementioned Kondo lattice of single-ion Kondo-like behavior, AFM and other types of order of the Sm ions, RKKY interactions between Ce and Sm ions, crystalline electric field effects, atomic disorder, etc. These

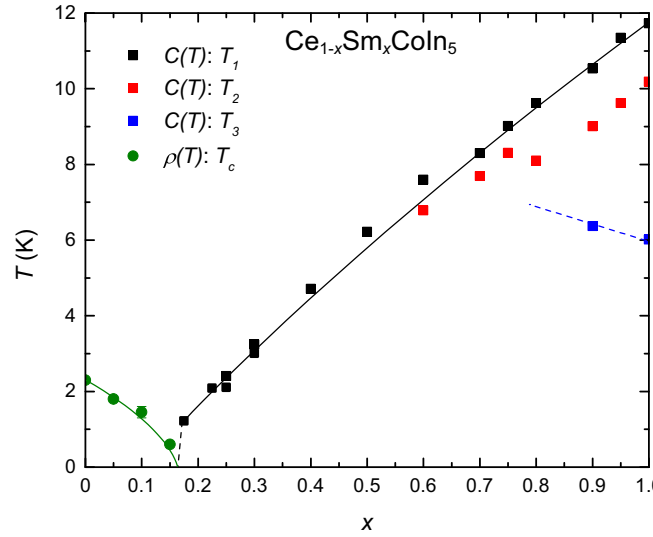

FIG. 4. Superconducting critical temperature, T_c, and Sm ordering temperatures T_1, T_2, and T_3 (where T_1 is the Néel temperature, T_N) vs Sm concentration, x. Lines are guides to the eye.

effects are highly sensitive to the Ce to Sm ratio which may vary somewhat throughout a $Ce_{1-x}Sm_xCoIn_5$ single crystal. For $x \geqslant 0.7$, the Ce^{3+} ion concentration is so dilute that a coherent Kondo lattice can no longer form, which explains the absence of a coherence peak for $x \geqslant 0.7$. Instead, a minimum followed by an upturn in $\rho(T)$ with decreasing temperature is observed as shown in Fig. 3(b). This behavior is reminiscent of the single-ion Kondo effect associated with a moderately dilute concentration of Ce^{3+} ions dissolved into $SmCoIn_5$. The RKKY interaction dominates for $x \geqslant 0.9$, which leads to long-range magnetic ordering of Sm^{3+} ions.

C. Magnetization

Magnetization measurements were performed on single crystals in the $Ce_{1-x}Sm_xCoIn_5$ system with an applied magnetic field $H = 5$ kOe oriented parallel to the ab plane; $M(T)/H$ data are shown in Fig. 5 for representative samples. This behavior is consistent with a Curie-Weiss law, shown in Eq. (1), for temperatures above ~50 K.

$$\frac{M}{H} = \frac{C}{T - \theta_{\mathrm{CW}}}. \tag{1}$$

It is challenging to perform a Curie-Weiss analysis of our M/H data since we have two distinct magnetic species with an easy axis along the c axis [7] on the Ce-rich side and perpendicular to the c axis [11] on the Sm-rich side. These issues along with the likelihood of the samples hosting minor amounts of magnetic impurities contribute to the magnetic susceptibility's nonmonotonic behavior with x. Therefore, we are unable to provide a detailed analysis of the evolution of the effective magnetic moment, μ_{eff}, and Curie-Weiss temperature, θ, with Sm concentration x.

A Curie-Weiss analysis of the $M(H,T)$ data for $SmCoIn_5$ is shown in Fig. 6. This analysis yielded an effective magnetic moment $\mu_{\mathrm{eff}} = 1.00\mu_B$ and a Curie-Weiss temperature $\theta = -73$ K. The value of μ_{eff} for Sm is slightly larger than the

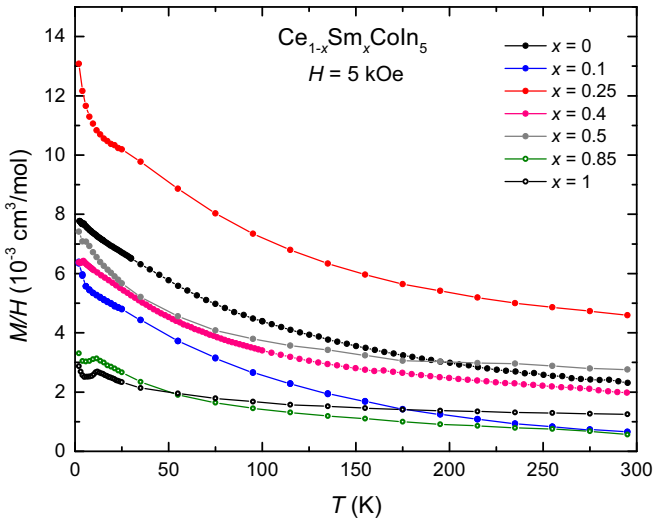

FIG. 5. Magnetization, M/H, vs temperature, T, measured in an applied magnetic field $H = 5$ kOe. The magnetic field was oriented parallel to the ab plane.

Sm^{3+} free ion Hund's rule value of $0.84\mu_B$ [29]. A negative value for θ reflects the influence of AFM interactions and the Van Vleck temperature-independent contribution to $\chi(T)$.

D. Specific heat

Specific heat measurements from 2 to 30 K are shown in Fig. 7. Additional measurements down to 0.5 K were also performed for selected samples with concentrations near the concentration where T_N is completely suppressed (AFM QCP) to look for NFL behavior. Data for $Ce_{1-x}Sm_xCoIn_5$ and $LaCoIn_5$ single crystals for $T > 30$ K are similar, particularly the T^2 dependence of C/T which suggests that $LaCoIn_5$ is a suitable nonmagnetic reference compound due to the similarity in the phonon contribution to the specific heat. The superconducting transition in $CeCoIn_5$ is observed with a sharp

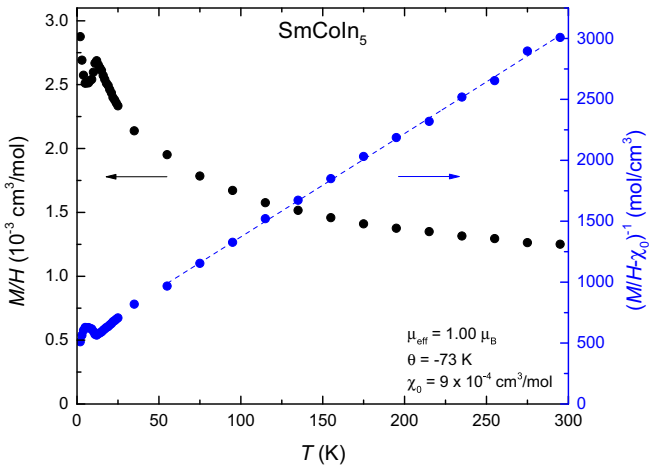

FIG. 6. Magnetization, M/H, and $(M/H - \chi_0)^{-1}$, where χ_0 is a constant, vs temperature, T, for $SmCoIn_5$. Best-fit values for the effective magnetic moment, μ_{eff}, Curie-Weiss temperature, θ, and χ_0 were extracted from a fit of the Curie-Weiss law to the data and are given in the panel. Features corresponding to magnetic transitions are observed at low temperatures.

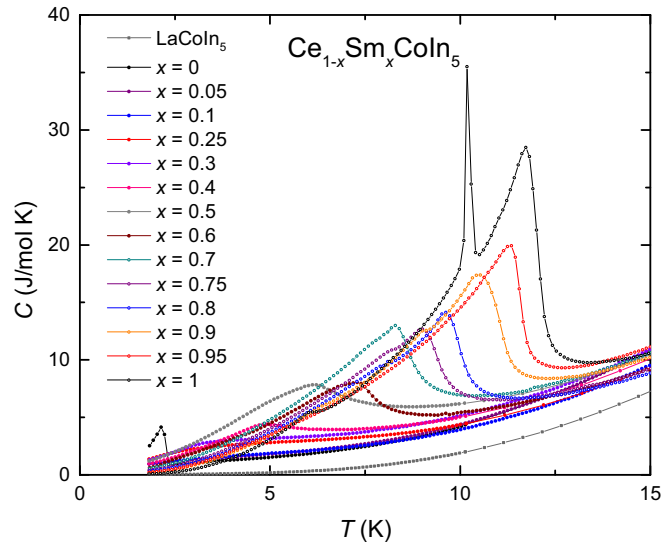

FIG. 7. Specific heat, C, vs temperature, T, between 2 and 30 K for $Ce_{1-x}Sm_xCoIn_5$ and a nonmagnetic reference compound, $LaCoIn_5$.

jump at $T_c = 2.3$ K. For Sm-rich compounds, we can identify up to three different phase transitions which are consistent with electrical resistivity and magnetization measurements as shown in Fig. 8; these transitions are likely associated with

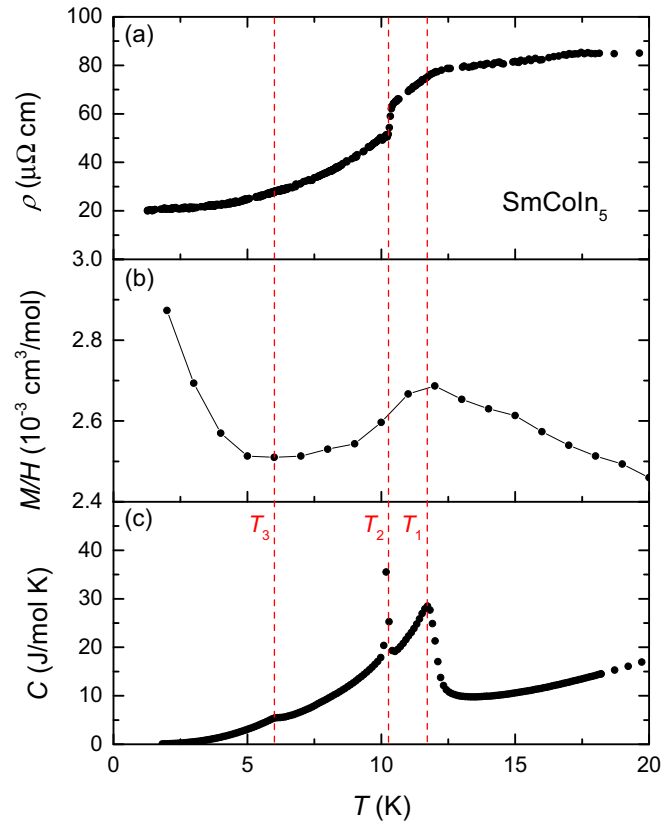

FIG. 8. (a) Electrical resistivity, ρ, (b) magnetization divided by magnetic field, M/H, and (c) specific heat, C, vs temperature, T, in the range $0 \leqslant T \leqslant 20$ K. Corresponding magnetic transitions can be observed in the different measurements with the vertical red dashed lines drawn through T_1, T_2, and T_3 which serve as guides to the eye.

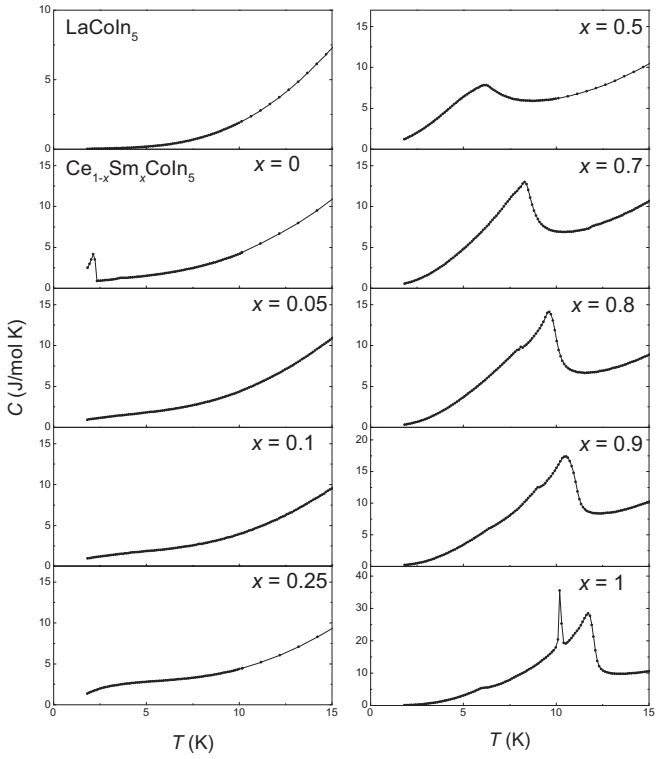

FIG. 9. Specific heat, C, plotted vs temperature, T, for $LaCoIn_5$ and $Ce_{1-x}Sm_xCoIn_5$ ($x = 0$, 0.05, 0.25, 0.5, 0.7, 0.8, 0.9, and 1) to demonstrate the evolution of behavior; we move from superconductivity on the Ce-rich side to antiferromagnetic order on the Sm-rich side.

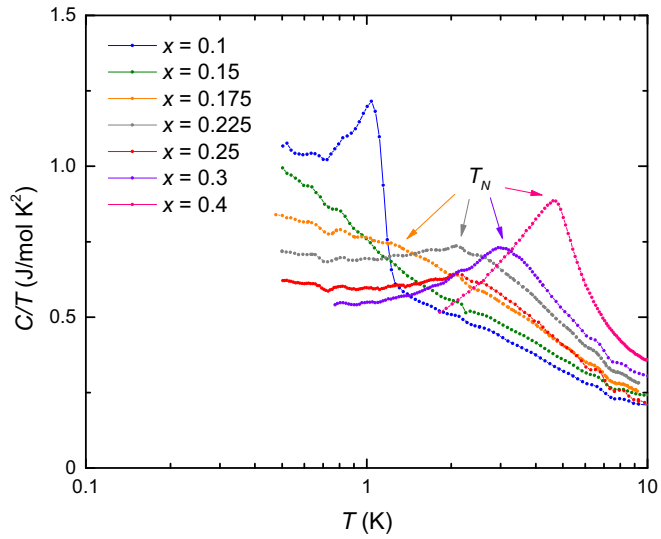

FIG. 10. Specific heat, C, divided by temperature, T, C/T, vs $\log(T)$ for selected Sm concentrations x near a potential AFM QCP. $C(T)/T$ exhibits a logarithmic divergence in T for $x = 0.15$, behavior that is consistent with quantum criticality. For other concentrations ($x = 0.1$, 0.175, 0.225, 0.25, 0.3, and 0.4), this behavior is not as apparent due to the proximity to their respective phase transitions, distance from the QCP, and the limited temperature range over which logarithmic behavior in T can be identified.

magnetic order, but two of them are currently unidentified as will be discussed later. The evolution of the specific heat data as we move from $x = 0$ to $x = 1$ is shown in Fig. 9 (where data for $LaCoIn_5$ are included for reference). These data were used to construct the phase diagram displayed in Fig. 4.

The highest transition temperature, T_1, is the Néel temperature, T_N, as reported by Inada *et al.* [11]. As we substitute Ce into $SmCoIn_5$, we observe a continuous suppression of T_1 down to $x = 0.175$. The second temperature, T_2, is also suppressed; however, it is not suppressed at the same rate as T_1, which eventually leads to an overlap of both transition signatures. This coincidence of features indicates either that we have only one distinct transition for these concentrations, or that they cannot be separately resolved by specific heat measurements. The third characteristic temperature, T_3, only appears as a very subtle feature in the data for both $x = 0.9$ and 1 (see Fig. 8). For all other concentrations (including $x = 0.95$), the feature at T_3 is either too small to detect, or it disappears. It is also possible that, like T_2, this transition merges with the other magnetic transitions. As seen in the phase diagram, T_3 appears to increase with decreasing x.

Three distinct transitions have been observed in other Sm-based members of the $Sm_nM_mIn_{3n+2m}$ family of compounds (M = Rh or Ir; $n = 1,2$; $m = 0,1$), such as $SmIn_3$, $SmIrIn_5$, $SmRhIn_5$, Sm_2IrIn_8, and Sm_2RhIn_8 [24,30,31]. It is particularly instructive to consider the compound $SmIn_3$, which is closely related to $SmCoIn_5$ (in analogy with the well-known structural relationship between $CeIn_3$ and $CeCoIn_5$). Muon spin rotation (μSR) measurements have been performed on $SmIn_3$ to clarify the nature of the three phase transitions; the results of this study demonstrated they are all associated with magnetic ordering [30]. From specific heat data [24], we see similar features indicative of phase transitions. We conclude that $SmCoIn_5$ and $SmIn_3$ each exhibit a similar AFM transition at their highest transition temperature, T_1. The nature of the remaining two transitions at T_2 and T_3 is still unknown. From the aforementioned study on $SmIn_3$ [25], there is evidence of a transition from incommensurate to commensurate AFM order at T_2; although, the shape of the specific heat feature is qualitatively different from our data presented herein. In either case, the nature of T_3 is still unknown. Additional measurements such as anomalous x-ray diffraction will need to be conducted to identify the nature of these ordered phases.

Heat capacity measurements were performed down to 0.5 K to characterize the $Ce_{1-x}Sm_xCoIn_5$ system around the potential AFM QCP. Figure 10 shows $C(T)/T$ data plotted on a semilogarithmic scale for selected concentrations in the vicinity of the possible QCP near $x = 0.15$. Consistent with NFL behavior, $C(T)/T$ for $x = 0.15$ diverges logarithmically with decreasing T over a large temperature range. Neighboring concentrations do not exhibit this strong logarithmic divergence in T due to the higher values of T_c ($x = 0.1$) and T_N ($x = 0.175$, 0.225, 0.25, 0.3, and 0.4), restricting the range within which NFL behavior can reasonably be distinguished. This picture is consistent with the current phase diagram in Fig. 4. As we see from our measurements, SC is observed up to a concentration $x = 0.1$ where $T_c \approx 1$ K and AFM is last observed at $x = 0.175$ below $T_N \approx 1.2$ K. Despite performing measurements down to 0.5 K, we were unable to observe any additional phase transitions at the concentration $x = 0.15$. The suppression of T_c and T_N with x becomes

nonlinear in this concentration range; instead, SC is suppressed much more rapidly with x for $x > 0.1$, while AFM order is suppressed more rapidly with decreasing x for $x < 0.175$. From this picture, we suggest that a QCP, associated with the suppression of both the SC and AFM phases where T_c and T_N are driven to zero temperatures, lies in very close proximity to the concentration $x = 0.15$.

The apparent AFM QCP at $x_{QCP} \approx 0.15$ for $Ce_{1-x}Sm_xCoIn_5$ reveals a gradual suppression of T_N with decreasing x in comparison to other substituted 115 compounds in which the AFM QCP occurs at larger values of x, such as $CeCo_{1-x}Rh_xIn_5$ [32,33] ($x_{QCP} \approx 0.25$), $Y_{1-x}Ce_xRhIn_5$ [26] ($x_{QCP} \approx 0.65$), and $La_{1-x}Ce_xRhIn_5$ [34] ($x_{QCP} \approx 0.5$). This may suggest a robust AFM phase in $SmCoIn_5$, supported by evidence of three distinct magnetic transitions, when compared to the AFM phase in $CeRhIn_5$. The measurements reported herein do not provide any evidence for the coexistence of the superconducting and AFM phases associated with the Ce and Sm ions, respectively, in contrast to $CeCo_{1-x}Rh_xIn_5$ at ambient pressure, in which the Ce ions are responsible for both the SC and the AFM ordering. Thus, the $Ce_{1-x}Sm_xCoIn_5$ system may fall into the class of magnetically ordered superconductors which consist of a superconducting subsystem involving electrons associated with Ce ions that interact via the exchange interaction with a magnetically ordered subsystem consisting of the localized f electrons of the Sm ions. In these types of systems, SC has been found to coexist with AFM order and to be suppressed by ferromagnetic order of localized magnetic moments [35].

IV. DISCUSSION

A. Electronic and phonon contributions to specific heat

Further analysis was performed on the specific heat data for $Ce_{1-x}Sm_xCoIn_5$ using the Debye model, $C/T = \gamma + \beta T^2$. By fitting a straight line to the C/T vs T^2 data in the temperature range $T > T_N$, we extracted best-fit values for β. We used the values of β to calculate the values of the characteristic Debye temperature, Θ_D, using the relation

$$\beta = \frac{12\pi^4 N_A k_B}{5\Theta_D^3}. \tag{2}$$

These results are plotted in Fig. 11 where Θ_D increases monotonically with x. Due to the broad features from magnetic ordering and the limited temperature range in which the Debye model is applicable, characterized by the calculated Debye temperature, it is difficult to extrapolate meaningful values of γ. We looked at two characteristic "γ" values as a general observation, one at 15 K and another at 2 K to compare to the value ($\gamma = 53\,\mathrm{mJ/mol\,K^2}$) from a study of $SmCoIn_5$ by Inada *et al.* [11]. To do this, we extracted values for C_e/T at 2 K, where $C_e/T \equiv C/T - \beta T^2$ is the electronic contribution to the specific heat divided by temperature; we performed a similar analysis above the magnetic ordering temperature by selecting C_e/T at 15 K. The results for C_e/T are plotted in Fig. 11, where we observe that values for C_e/T at high and low T behave in opposite manners; at 2 K, the value of C_e/T simply decreases with x for $x \geqslant 0.25$ (concentrations where the AFM transition is clearly observed). This trend can be

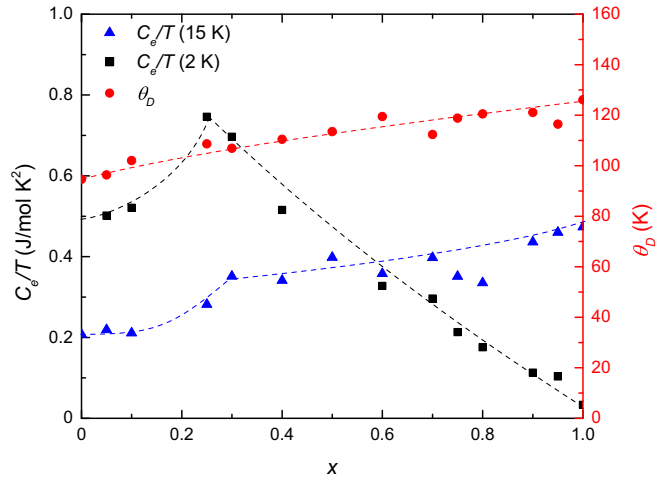

FIG. 11. Electronic contribution to the specific heat divided by temperature, C_e/T, at 2 K (black squares), temperature-independent contribution to C_e/T at 15 K, above the magnetic ordering temperature (blue triangles), and Debye temperature Θ_D (red circles), all plotted as a function of Sm concentration x, in $Ce_{1-x}Sm_xCoIn_5$. Dashed curves are guides to the eye. The procedures for determining the values of C_e/T at 2 and 15 K are described in the text.

easily understood since the closer T_N is to 2 K, the larger the magnetic contribution is to C_e/T. For C_e/T at 15 K (a high-temperature, normal-state γ), we observe a similar trend with x as we did at 2 K for $x < 0.25$; however, for $x \geqslant 0.25$, there is a monotonic increase in C_e/T due to the introduction of the AFM transition above $x = 0.225$.

B. Entropy calculations from specific heat

Entropy calculations were made using measured specific data via numerical integration of Eq. (3).

$$S(T) = \int \frac{C_e(T)}{T} dT. \tag{3}$$

Calculations of $S(T)$ associated with magnetic ordering are compared to various values of the entropy $R\ \ln(2J+1)$ in Fig. 12 with dashed lines for $J = \frac{1}{2}$, 1, and $\frac{3}{2}$. Concentrations exhibiting large peaks in C vs T data ($x \geqslant 0.5$) show a change in slope near characteristic entropy values. For $0.5 \leqslant x \leqslant 0.8$, the entropy associated with magnetic ordering is around $R\ \ln 2$. For Sm-rich concentrations ($x \geqslant 0.9$), the change in entropy is about $R\ \ln 3$; we have already described a crossover in behavior of the electrical resistivity data that also occurs near $x \approx 0.9$ (see Fig. 3).

C. Non-Fermi-liquid behavior in low-temperature electrical resistivity

Low-temperature electrical resistivity, $\rho(T)$, data in the paramagnetic state are often fitted using a power-law function of the usual form:

$$\rho = \rho_0 + AT^n. \tag{4}$$

Due to errors in the geometrical factor A/L (A = cross-sectional area, L = length) used to convert electrical resistance R to electrical resistivity $\rho = R(\frac{A}{L})$, the following equation

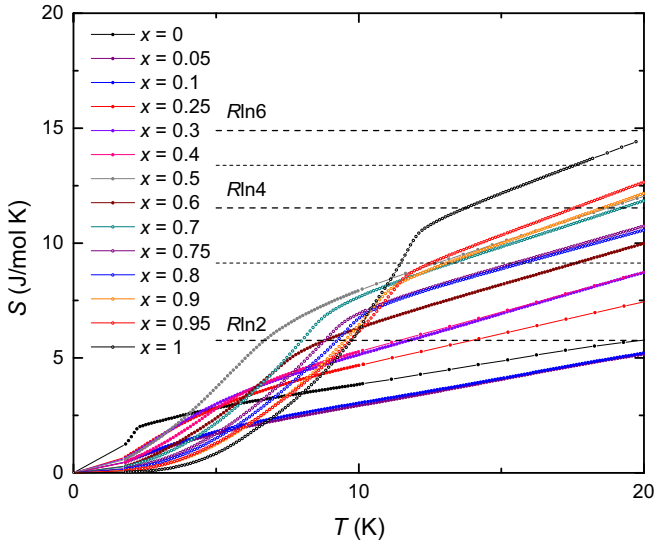

FIG. 12. Electronic entropy, $S(T)$, calculated as described in the text, plotted vs temperature, T. Dashed lines showing $R\ln(2J+1)$ at various values of total angular momentum J are provided for comparison.

was fitted to the normalized resistivity, $\rho(x,T)/\rho(300\text{ K})$, data:

$$(\rho-\rho_0)/\rho(300\text{ K}) = A'T^n, \tag{5}$$

where $A' = A/\rho(300\text{ K})$.

Exponents, n, that are subquadratic, indicative of NFL behavior, were observed to develop in the $0 \leqslant x \leqslant 0.5$ concentration region. This fitting procedure is reasonable around the projected QCP near $x = 0.15$; however, due to the proximity to the superconducting and magnetically ordered phases, the temperature range in which this fit can be achieved is very small. By plotting $\log[(\rho-\rho_0)/\rho(300\text{ K})]$ vs $\log T$ (see Fig. 13), we observed a linear region which corresponds to a constant value of n. Extracting n as the slope of the line in these plots, we plotted $\rho_0/\rho(300\text{ K})$, A', and n vs x to characterize the

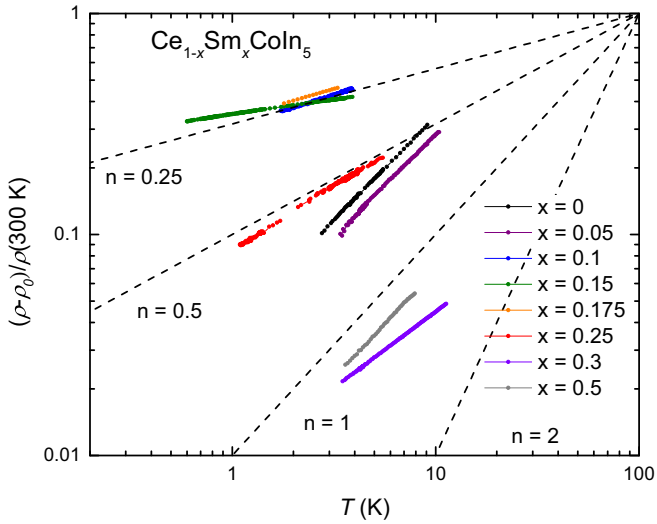

FIG. 13. Plot of $\log[(\rho-\rho_0)/\rho(300\text{ K})]$ vs $\log T$ for $Ce_{1-x}Sm_xCoIn_5$ ($0 \leqslant x \leqslant 0.5$) up to $T \approx 15$ K. Linear behavior indicates power-law behavior given by Eq. (5). Dashed lines are provided at exponents of $n = 0.5$, 1, and 2 as guides to the eye.

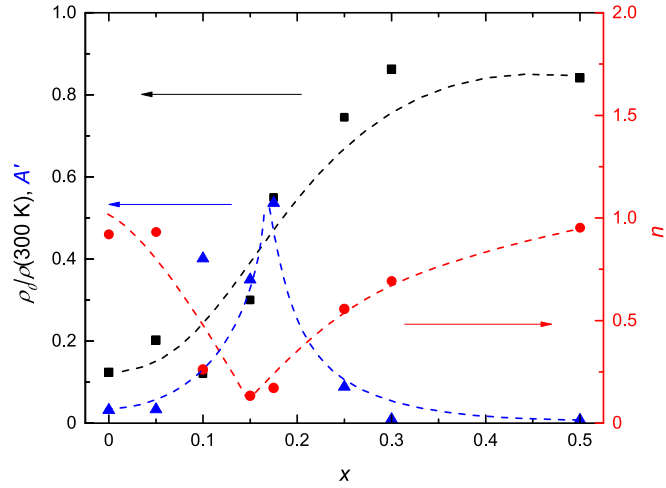

FIG. 14. Normalized residual resistivity $\rho_0/\rho(300\text{ K})$ (black), normalized coefficient A' (blue), and exponent n (red) vs Sm concentration x for $Ce_{1-x}Sm_xCoIn_5$. The values of $\rho_0/\rho(300\text{ K})$, A', and n were extracted from fits of Eq. (5) to the $\rho(x,T)$ data in Fig. 13.

behavior of the electrical resistivity around the QCP as shown in Fig. 14. We observe a decreasing NFL exponent of $n \approx 1$ at $x = 0$ to $n \approx 0.13$ at $x = 0.15$ before n returns to $n \approx 1$ as x increases beyond the QCP near $x = 0.15$. The normalized residual resistivity, $\rho_0/\rho(300\text{ K})$, increases steadily as a function of x, likely due to the increasing number of magnetic ions introduced via Sm substitution. The normalized coefficient, $A'(x)$, shows a sharp cusp near the QCP, which is indicative of NFL behavior. The behavior of $n(x)$ is consistent with quantum critical behavior where proximity to a QCP in the normal state results in a departure of the physical properties from Fermi-liquid behavior where $n = 2$. The residual resistivity, $\rho_0(x)$, and the coefficient, $A(x)$, can be determined by multiplying the normalized residual resistivity, $\rho_0(x)/\rho(x,300\text{ K})$, and normalized coefficient, $A'(x) = A(x)/\rho(x,300\text{ K})$, by the value of $\rho(x,300\text{ K})$ determined by making a least-squares fit of the relation $\rho(x,300\text{ K}) = \rho(0,300\text{ K}) + \alpha x$ to the $\rho(x,300\text{ K})$ data. This fit yields the values $\rho(0,300\text{ K}) = 0.21 \pm 0.19$ mΩ cm and $\alpha = 2.23 \pm 0.80$ mΩ cm. The errors reflect the scatter in the measured values of $\rho(x,300\text{ K})$, which are partially due to uncertainties in the geometrical factor used to convert $R(T)$ to $\rho(T)$.

The power-law behavior of the electrical resistivity in this system is consistent with a previous study of other $Ce_{1-x}R_xCoIn_5$ systems (R = Yb, Y, Lu, Er, Dy, Gd) by Paglione *et al.* [36], in which values of $n \lesssim 1$ were found for various R substituents. Furthermore, an inverse proportionality between n and ρ_0 for each R ion was found, similar to what we have observed in the $Ce_{1-x}Sm_xCoIn_5$ system.

V. CONCLUDING REMARKS

Based on powder x-ray diffraction, electrical resistivity, magnetization, and specific heat measurements on $Ce_{1-x}Sm_xCoIn_5$ single crystals, we constructed a T vs x phase diagram for this system. As Sm is substituted for Ce, we observe a crossover from superconductivity on the Ce-rich side to antiferromagnetism and other types of order whose origin is currently unknown on the Sm-rich side. We observed NFL

behavior consistent with quantum criticality in the intermediate region $0.1 < x < 0.225$. There appears to be an AFM QCP in the vicinity of $x = 0.15$ with no indication of coexistence of SC and AFM. An evolution from Kondo coherence to single-ion Kondo behavior and then eventually to magnetic ordering via the RKKY interaction (and other types of order) occurs as x increases from 0 to 1. Since Sm has a high neutron absorption cross section making it unsuitable for neutron-scattering measurements, further studies into this compound using techniques such as anomalous x-ray diffraction will be necessary to elucidate the nature of magnetic order in the $Ce_{1-x}Sm_xCoIn_5$ system.

ACKNOWLEDGMENTS

Research at the University of California, San Diego was supported by the US Department of Energy, Office of Basic Energy Sciences, Division of Materials Science and Engineering under Grant No. DE-FG02-04-ER46105 (materials synthesis and characterization) and the US National Science Foundation under Grant No. DMR-1206553 (low-temperature measurements). Research at Kent State University was supported by the US National Science Foundation under Grant No. DMR-1505826 (low-temperature specific heat measurements).

[1] P. Gegenwart, Q. Si, and F. Steglich, Nature Phys. **4**, 186 (2008).
[2] F. Steglich, J. Arndt, S. Friedemann, C. Krellner, Y. Toskiwa, T. Westerkamp, M. Brando, P. Gegenwart, C. Geibel, S. Wirth, and O. Stockert, J. Phys.: Condens. Matter **22**, 164202 (2010).
[3] J. D. Thompson and Z. Fisk, J. Phys. Soc. Jpn. **81**, 011002 (2012).
[4] G. Stewart, Rev. Mod. Phys. **56**, 755 (1984).
[5] F. Steglich, C. Geibel, R. Modler, M. Lang, P. Hellmann, and P. Gegenwart, J. Low Temp. Phys. **99**, 267 (1995).
[6] B. D. White, J. D. Thompson, and M. B. Maple, Physica C **514**, 246 (2015).
[7] C. Petrovic, P. G. Pagliuso, M. F. Hundley, R. Movshovich, J. L. Sarrao, J. D. Thompson, and Z. Fisk, J. Phys.: Condens. Matter **13**, L337 (2001).
[8] L. H. Greene, W. K. Park, J. L. Sarrao, and J. D. Thompson, Physica B **378**, 671 (2006).
[9] B. B. Zhou, S. Misra, E. H. da Silva Neto, P. Aynajian, R. E. Baumbach, J. D. Thompson, E. D. Bauer, and A. Yazdani, Nat. Phys. **9**, 474 (2013).
[10] M. P. Allan, F. Massee, D. K. Morr, J. Van Dyke, A. W. Rost, A. P. Mackenzie, C. Petrovic, and J. C. Davis, Nat. Phys. **9**, 468 (2013).
[11] Y. Inada, M. Hedo, T. Fujiwara, T. Sadamasa, and Y. Uwatoko, Physica B **378**, 421 (2006).
[12] M. Koeda, M. Hedo, T. Fujiwara, Y. Uwatoko, T. Sadamasa, and Y. Inada, J. Phys. Soc. Jpn. **76**, 62 (2007).
[13] E. D. Bauer, M. M. Altarawneh, P. H. Tobash, K. Gofryk, O. E. Ayala-Valenzuela, J. N. Mitchell, R. D. McDonald, C. H. Mielke, F. Ronning, J.-C. Griveau, E. Colineau, R. Eloirdi, R. Caciuffo, B. L. Scott, O. Janka, S. M. Kauzlarich, and J. D. Thompson, J. Phys.: Condens. Matter **24**, 052206 (2012).
[14] L. Shu, R. E. Baumbach, M. Janoschek, E. Gonzales, K. Huang, T. A. Sayles, J. Paglione, J. O'Brien, J. J. Hamlin, D. A. Zocco, P.-C. Ho, C. A. McElroy, and M. B. Maple, Phys. Rev. Lett. **106**, 156403 (2011).
[15] C. Capan, G. Seyfarth, D. Hurt, B. Prevost, S. Roorda, A. D. Bianchi, and Z. Fisk, Europhys. Lett. **92**, 47004 (2010).
[16] L. Dudy, J. D. Denlinger, L. Shu, M. Janoschek, J. W. Allen, and M. B. Maple, Phys. Rev. B **88**, 165118 (2013).
[17] T. Hu, Y. P. Singh, L. Shu, M. Janoschek, M. Dzero, M. B. Maple, and C. C. Almasan, Proc. Natl. Acad. Sci. **110**, 7160 (2013).
[18] A. Polyakov, O. Ignatchik, B. Bergk, K. Götze, A. D. Bianchi, S. Blackburn, B. Prévost, G. Seyfarth, M. Côté, D. Hurt, C. Capan, Z. Fisk, R. G. Goodrich, I. Sheikin, M. Richter, and J. Wosnitza, Phys. Rev. B **85**, 245119 (2012).
[19] H. Kim, M. A. Tanatar, R. Flint, C. Petrovic, R. Hu, B. D. White, I. K. Lum, M. B. Maple, and R. Prozorov, Phys. Rev. Lett. **114**, 027003 (2015).
[20] Y. Xu, J. K. Dong, I. K. Lum, J. Zhang, X. C. Hong, L. P. He, K. F. Wang, Y. C. Ma, C. Petrovic, M. B. Maple *et al.*, Phys. Rev. B **93**, 064502 (2016).
[21] O. Erten, R. Flint, and P. Coleman, Phys. Rev. Lett. **114**, 027002 (2015).
[22] M. Shimozawa, T. Watashige, S. Yasumoto, Y. Mizukami, M. Nakamura, H. Shishido, S. K. Goh, T. Terashima, T. Shibauchi, and Y. Matsuda, Phys. Rev. B **86**, 144526 (2012).
[23] S. Jang, B. D. White, I. K. Lum, H. Kim, M. A. Tanatar, W. E. Straszheim, R. Prozorov, T. Keiber, F. Bridges, L. Shu, and R. E. Baumbach, Philos. Mag. **94**, 4219 (2014).
[24] M. Kasaya, B. Liu, M. Sera, T. Kasuya, D. Endoh, T. Goto, and T. Fujimura, J. Magn. Magn. Mater. **52**, 289 (1985).
[25] T. U. Ito, W. Higemoto, K. Ninomiya, H. Luetkens, T. Sugai, Y. Haga, and H. S. Suzuki, J. Magn. Magn. Mater. **80**, 033701 (2011).
[26] V. S. Zapf, N. A. Frederick, K. L. Rogers, K. D. Hof, P.-C. Ho, E. D. Bauer, and M. B. Maple, Phys. Rev. B **67**, 064405 (2003).
[27] A. C. Larson and R. B. von Dreele, General Structure Analysis System (GSAS), Los Alamos National Laboratory Report LAUR 86-748 (1994).
[28] H. M. Rietveld, J. Appl. Crystallogr. **2**, 65 (1969).
[29] J. H. Van Vleck, *The Theory of Electric and Magnetic Susceptibilities* (Oxford University Press, New York, 1932).
[30] Takashi U. Ito, W. Higemoto, K. Ninomiya, H. Luetkens, T. Sugai, Y. Haga, and H. S. Suzuki, J. Phys. Soc. Jpn. **80**, 033710 (2011).
[31] P. G. Pagliuso, J. D. Thompson, M. F. Hundley, J. L. Sarrao, and Z. Fisk, Phys. Rev. B **63**, 054426 (2001).
[32] V. S. Zapf, E. J. Freeman, E. D. Bauer, J. Petricka, C. Sirvent, N. A. Frederick, R. P. Dickey, and M. B. Maple, Phys. Rev. B **65**, 014506 (2001).
[33] J. R. Jeffries, N. A. Frederick, E. D. Bauer, H. Kimura, V. S. Zapf, K.-D. Hof, T. A. Sayles, and M. B. Maple, Phys. Rev. B **72**, 024551 (2005).
[34] B. E. Light, R. S. Kumar, A. L. Cornelius, P. G. Pagliuso, and J. L. Sarrao, Phys. Rev. B **69**, 024419 (2004).
[35] M. B. Maple, Physica B **215**, 110 (1995).
[36] J. Paglione, T. A. Sayles, P.-C. Ho, J. R. Jeffries, and M. B. Maple, Nat. Phys. **3**, 703 (2007).